Integrated Ferroelectrics, 1998, Vol. 19, pp. 121 – 140
Reprints available directly from the publisher
Photocopying permitted by license only

ANALYSIS OF PREFERRED ORIENTATIONS IN PST AND PZT THIN FILMS ON VARIOUS SUBSTRATES

D. CHATEIGNER[a,b,**], H.-R. WENK[a,b], A. PATEL[c], M. TODD[d] and D. J. BARBER[e,*]

[a]*Laboratoire de Cristallographie-CNRS, BP 166, 38042 Grenoble, France;* [b]*Department of Geology and Geophysics, Univ. of California, Berkeley CA 94720, USA;* [c]*GEC-Marconi Materials Technology Limited, Northamptonshire NN12 8EQ, U. K;* [d]*Defence Research Agency, Malvern, Worcestershire, U. K;* [e]*Department of physics, Hong Kong Univ. of Science and Technology, Hong Kong*

Orientation distributions of Pb(Zr, Ti)O_3 and Pb_2ScTaO_6 thin films deposited on various substrates and buffer layers are described. All observed textures are basically fibre textures.Only PST films deposited on MgO/(11$\bar{2}$0)-Al_2O_3 show a weak in-plane alignment, with ⟨100⟩ PST perpendicular to the film surface. PST films deposited on a Pt/(100)-Si substrate exhibit a strong ⟨111⟩ fibre texture, tilted 5° to the normal. The Pt substrate has also a ⟨111⟩ fibre texture, with orientation densities as high as 60 times the random distribution (m.r.d.). On both substrates, PST films show maxima in the orientation distribution near 35 m.r.d.

PZT films (PZT/Pt/Si-(100) and PZT/Pt/Ti/SiO_2/Si-(100)) have a ⟨111⟩ fibre texture. The maximum orientation distribution observed for PZT is 200 m.r.d. A minor ⟨100⟩ fibre component may be present. The Pt textures resemble qualitatively those of PZT, mainly ⟨111⟩. The addition of a Ti buffer layer on grown SiO_2 favors the stabilization of PZT in a tetragonal crystal system, and increases strongly the Pt texture, and to a lesser degree that of PZT.

Keywords: Ferroelectrics; texture; thin films; PST; PZT; orientation distribution

INTRODUCTION

The preparation and processing methods used to fabricate thin films should give control over their microstructure and ideally they should enable

**Corresponding author.
*Now at School of Industrial and Manufacturing Science, Cranfield Univ., Cranfield, Bedfordshire MK430AL, U. K.

optimization of the properties of the films for specific device applications. Epitaxial films with a high degree of preferred orientation are often needed. Close lattice matching between the substrate and deposited material is generally utilised to achieve strongly crystallographically-oriented films, using many different techniques. Results on various types of superconducting oxides and ferroic materials feature most prominently in the literature.

Lead zirconate titanate, $PbZr_xTi_{1-x}O_3$ (PZT) and PLZT (PZT with some La substituted for Pb) thin films are of great technological interest on account of their unique and diverse electrical and optical responses to the application of an electric field. Applications include non-volatile ferroelectric RAM, capacitive elements in Integrated Circuits, and electro-optic devices. PST (lead scandium tantalate) has attracted much less attention, but it is one of the prime materials for use in uncooled pyroelectric infrared detectors, on account of its performance.

Much attention has been given to the growth of oxide films on substrates and to the structures of the resulting interfaces. However, there is scant data on films which merely have a strong preferred orientation, on the factors which influence it and on its quantitative influence on physical properties. Most researchers have deemed it sufficient to examine the intensities of the X-ray peaks for one or two specific reflections which are characteristic in certain cases of a given texture. Some exceptions are in the superconductivity field for texture studies of YBCO thin films, as a function of deposition temperature [1] and its quantitative correlation to critical current densities.[2] The lack of detailed textural data is particularly true in the case of polycrystalline thin films of some important ferroelectric materials such a PZT, PLZT (La-doped PZT). For these materials the crystallisation, growth, and optimization of the perovskite phase has been widely followed by the intensities of major X-ray reflections [3, 4] and other more unusual indicators,[5] and numerous TEM and SEM studies were dedicated to the optimization of their dielectric properties through the elimination of pyrochlore and amorphous phases.[6, 7, 8] However, XRD methods have not been widely employed to obtain quantitative texture information.

EXPERIMENTAL

Sample Preparation and Description

Bulk Pb(Zr, Ti)O_3 (PZT) crystallises at room temperature in the tetragonal or rhombohedral crystal system depending on the composition, with unit-

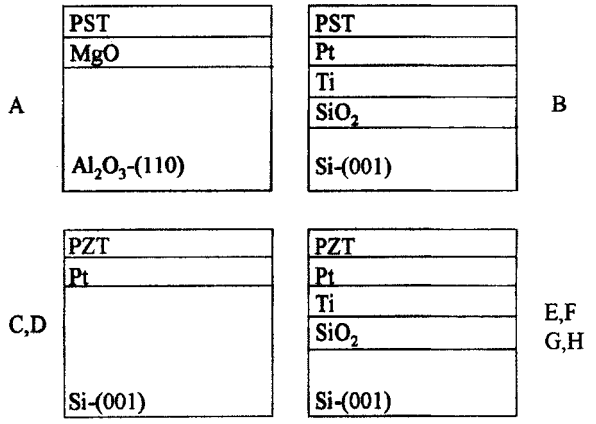

FIGURE 1 Schematic representation of samples A to H. Relative thickness are arbitrary. Since the SiO_2 buffer layer of samples C and D is the thin native oxide of the Si substrate, it is not represented.

cell parameters of $a=4.04$Å, $c=4.13$Å (tetragonal) and $a=4.08$Å, $\alpha=89.85°$ (rhombohedral). The high temperature phase is cubic. The PZT films C and D were deposited by a sol-gel route described previously.[9] The deposition procedure includes a drying process at low temperature after each layer is deposited and at the end of the deposition the whole sample is finally annealed. The PZT films E to H (Fig. 1, Tab. I) were fabricated by a sol-gel route. [10] For these four specimens, a rapid annealing was operated after each deposited layer at a temperature of 500–520°C inducing its crystallisation.

Pb_2ScTaO_6 (PST) is a cubic perovskite (Fm3m; $a=8.14$ Å) when in the paraelectric state, and undergoes a mild distortion to a rhombohedral

TABLE I Sample characteristics and preparation condtions. Due to the relatively weak PZT textures observed in samples C and D for similar conditions of preparation, no precise characterisation of these samples was pursued

Sample	*Sc/Ta or Zr/Ti*	*Stacking sequence*	*layer thicknesses (Å)*	*substrate*	*annealing temperature (°C)*
A	1/.97	PST/MgO	22000/3000	Al_2O_3-(11$\bar{2}$0)	550
B	1/.86	PST/Pt/Ti/SiO_2	18000/1000/100/8000	Si-(100)	550
C		PZT/Pt	–	Si-(100)	–
D		PZT/Pt	–	Si-(100)	–
E	25/75	PZT/Pt/Ti/SiO_2	10000/500/50/3800	Si-(100)	520
F	30/70	PZT/Pt/Ti/SiO_2	7000/1000/50/3800	Si-(100)	520
G	30/70	PZT/Pt/Ti/SiO_2	10000/500/50/3800	Si-(100)	520
H	30/70	PZT/Pt/Ti/SiO_2	10000/500/50/3800	Si-(100)	520

structure (R3 or R3m [11]) when ferroelectric below the Curie temperature. This latter varies with the degree of order of the Sc and Ta atoms, being 0°C for disordered PST and 26°C for the fully ordered phase. The PST films A and B investigated in this study, were prepared by RF sputtering using a multicomponent all-metal target,[12] and were crystallised rapidly at temperatures of 550°C. Such processing conditions do not give any structural order, the minimum temperature to induce ordering in PST being 600°C.[13]

For both these ferroelectric materials, the perovskite or deformed-perovskite crystal structure can be modified by their deposition as thin films, as results of substrate interactions and/or deposition conditions.

The samples used in this study consist of several layers (Fig. 1). One of the two PST films was sputtered onto a magnesium oxide buffer layer which had been deposited on a $(11\bar{2}0)$-Al_2O_3 single-crystal. The other PST film was sputtered onto Pt/Ti/SiO_2 on (100)-Si. The six PZT films were deposited on platinum films beneath which there were Ti and SiO_2 buffers on the Si substrates. For the four E to H samples, the SiO_2 layer was thermally grown oxide, while Pt/Ti was deposited using electron beam deposition. For the other two samples (C and D) the SiO_2 was native oxide and the Pt/Ti was sputter deposited. No annealing step was operated on these underlying layers before deposition of PZT by the spin-coating process. For PZTs only (100)-Si single-crystals have been used as substrates. Table I summarises the samples and preparation conditions. The textures of the Ti layers could not be measured because of the small thickness. The thermally formed SiO_2 phase was grown up to an estimated thickness of 3800Å and thought to be amorphous, like the native oxide. It was not investigated.

X-ray Diffraction

Both X-ray diffraction pole figures and θ-2θ diagrams were measured on a high resolution PTS Seifert goniometer, in reflection geometry[14] with $CuK_{\bar{\alpha}}$ radiation supplied by a rotating anode generator, and monochromatized by a 0002 graphite monochromator. Collimation and detecting slit apertures were fixed, with a peak width at half maximum of 0.08° in θ for the 400 silicon reflection ($\theta = 34.6°$).

With the Eulerian cradle of a pole figure goniometer (Fig. 2) the sample can be rotated into any arbitrary orientation. The goniometer rotations φ and χ correspond to azimuth and complement to the pole distance (α) in the pole figure. The recorded intensities at a given Bragg angle are proportional to the number of lattice planes {hkl} which are in reflection positions.

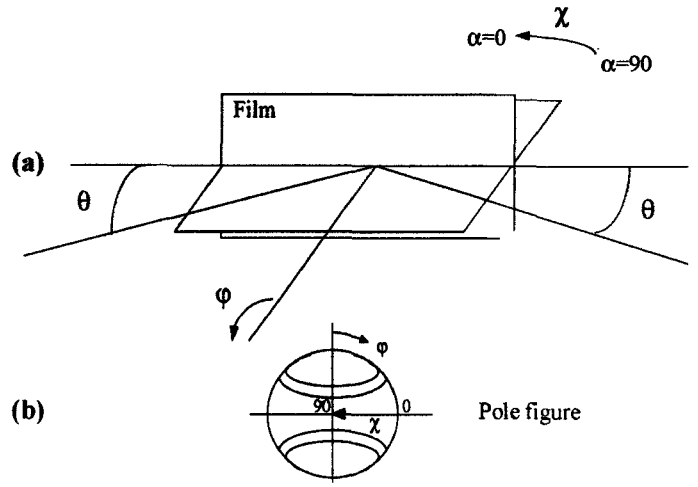

FIGURE 2 Definition of angles of the experimental set up (**a**), and their correspondence on pole figures (**b**) Intensities are projected on the film surface in the $\chi = 90°$ position.

θ-2θ scans were performed in the center of the pole figure ($\varphi = 0$, $90-\chi = 0$) in the range $2 \leq \theta \leq 60°$ in steps of 0.01°, with 10sec. of counting time. They were used to determine the Bragg peak positions for the pole figure measurements, and to refine lattice parameters of the PST and PZT films. Measured data were fitted with Gaussians. Systematic shifts in θ were corrected using the substrate peak positions. Lattice parameters were refined with a non-linear least square procedure (CELREF program[15]). θ-2θ patterns give also a first qualitative estimate for the texture type in the films. For instance, film A (Fig. 3b) shows a strong 400 peak and film B (Fig. 3b) a strong 222 peak indicative of corresponding alignment of lattice planes parallel to the surface. However such diagram do not reveal eventual in-plane orientations.

Experimental pole figures were first measured using angle increments of 5° in φ and χ, up to $90-\chi = 70°$, and with 10sec. counting time. If the raw data indicated a strong texture the scan was repeated using smaller increments (as small as 0.9° in χ and 1.8° in φ, up to $90-\chi = 72°$). In this case spline interpolation has been used to reconstruct a $5° \times 5°$ grid. Background and defocusing corrections, were done using a random standard. The correction curve was first modified to account for absorption and volume variations with sample tilt.[16, 17]

For a quantitative evaluation of the textures it is necessary to normalise the pole figures and express pole densities in multiples of a random

distribution (m.r.d.). A sample without any preferred orientation (or random sample) exhibits pole figures with constant density values of 1 m.r.d., while a textured sample shows pole figures with regions of densities above and below 1 m.r.d. As we measured only incomplete pole figures, a true normalisation could only be achieved through the orientation distribution (OD). The OD refinement from pole figures was done with the WIMV method.[18] The method as applied uses a discretised orientation space in $5° \times 5° \times 5°$ cells. It becomes less quantitative when the texture peak widths are in a similar range, as for the Pt layers in this study. The quality of the refined OD is checked by the RP and RP1 reliability factors [19] and by comparing experimental and recalculated pole figures. We also determined bulk parameters indicative of texture such as the "Texture Index" [20] and entropy.[21]

Pole figures are distributions of specific {hkl} planes relative to sample co-ordinates. We also calculated inverse pole figures which, particularly for

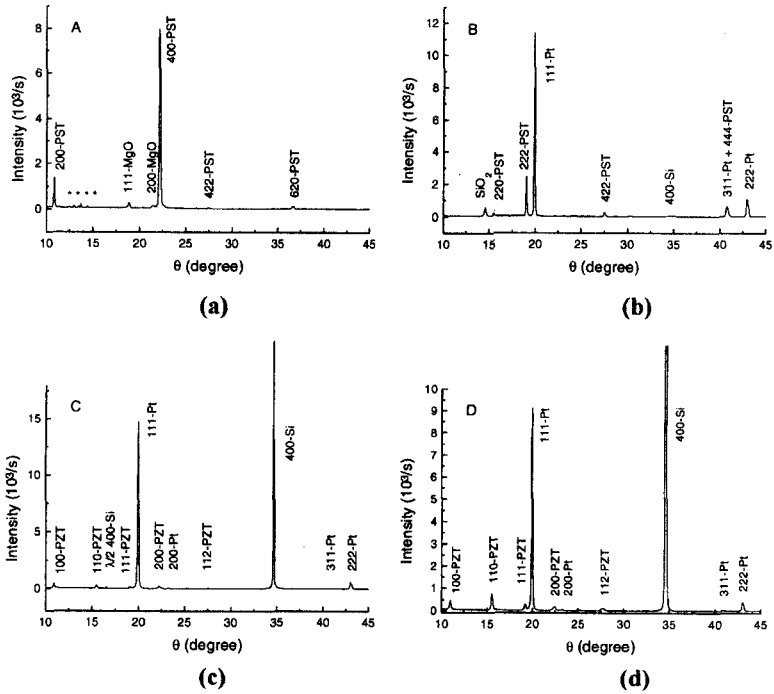

FIGURE 3 θ-2θ diagrams in the 10–45 degree range in θ. Intensities have been normalised to 1sec. of counting time. Substrate peaks are cut for clarity, * symbols stand for unknown parasitic phases.

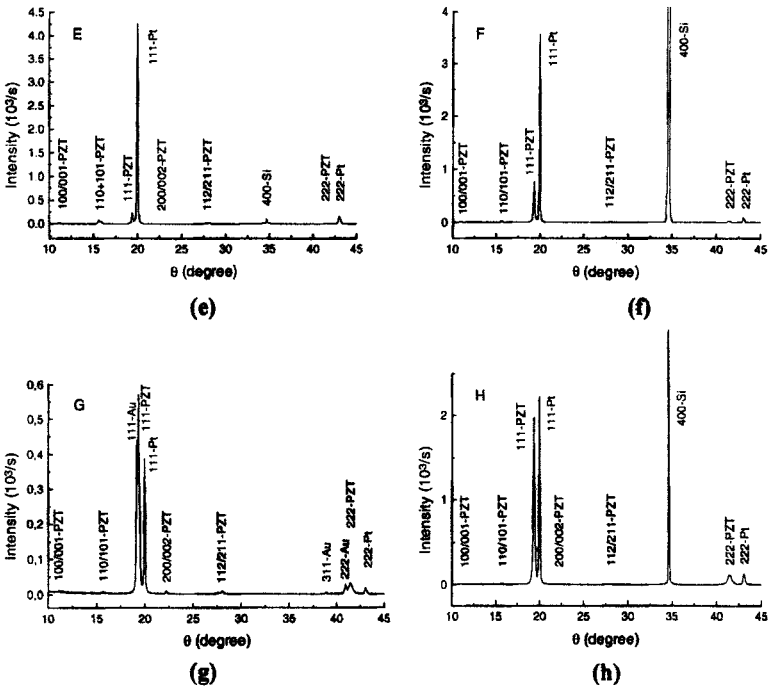

FIGURE 3 (Continued).

fibre texture with axial symmetry, are useful to identify and quantify texture components.

Normalisation, calculations of pole figures, OD and inverse pole figures were done with the Berkeley Texture Package (BEARTEX).[22] When the texture was extremely strong (Pt layers principally), we calculated the density of the {111} pole by integrating the direct intensities of the pole figures, using a local program (POFINT).

RESULTS

X-ray Diffraction Patterns

Figure 3 shows the XRD diagrams of our samples. The PST and PZT phases, MgO buffer layer, and recrystallized Pt substrates are clearly recognisable. Single crystal substrate peaks are not visible on all patterns, or only as weak components, because lattice planes are not in reflection

orientation, even for planes which supposedly are parallel to the surface. A diffraction peak may be visible on sample B, as a broad line (0.196° of half-width) centered at 3.06Å, which cannot be attributed to PST, Pt, Ti or Si. The SiO_2 buffer layer is generally thought to be amorphous, when it is a direct result of oxidation of the substrate surface. In our case this layer is specifically grown to limit interdiffusion, and the subsequent annealing of the sample may induce crystallisation. The 3.06Å d-spacing is well suited to crystalline SiO_2 phase. However, from only one peak we cannot attribute it to a specific SiO_2 phase. The Ti buffer layers are not detected. Sample A shows additional peaks but not in significant proportions. These possibly come from Pb rich phases, as this film has a Pb/Sc/Ta ratio of 3/1/0.97 as determined by electron probe microanalysis.

Table II lists the full width at half maxima (ω) of the diffraction peaks from PST and PZT films, and the refined cell parameters. Figure 4a illustrates the quality of fits on the 101/110 double component of sample E. Because of the strong preferred orientation some peaks were invisible. PST films exhibit the same widths (in the experimental resolution) as the platinum ($\theta_{111} = 19.954°$, $\omega = 0.125°$), indicating their relatively good crystalline state (absence of residual stresses and large crystallite sizes, in the experimental resolution). By contrast, PZT films have noticeably larger

TABLE II Peak positions, half widths and cell parameters of the PST and PZT films $\omega = 0.08°$ on 400 of Si, 0.125° on 111 of Pt. In parentheses the standard deviation of the least significant digit

		$\theta°$	$\omega°$	$\theta°$	$\omega°$	$\theta°$	$\omega°$	$\theta°$	$\omega°$		
	hkl	200		220		222		400		a(Å)	Rw (%)
PST	A	10.86	0.110	–	–	–	–	22.17	0.159	8.173(4)	0.24
	B	–	–	15.47	0.114	19.06	0.122	–	–	8.176(4)	0.24
	hkl	100		101 110		111		112 211		a(Å) c(Å)	
	C	10.90	0.144	15.50	0.154	19.11	0.187	27.56	0.296	4.080(2) –	0.14
	D	10.97	0.161	15.56	0.185	19.20	0.155	27.73	0.343	4.058(6) –	0.38
PZT	E	–	–	15.64 15.88	0.193 0.183	19.38	0.155	27.73 28.17	0.414 0.222	3.984(3) 4.099(4)	0.29
	F	–	–	–	–	19.32	0.177	27.64 28.06	0.431 0.244	3.997(4) 4.109(4)	0.32
	G	10.90	0.149	15.50 –	0.157 –	–	–	27.57	0.249	4.080(2) –	0.11
	H	–	–	–	–	19.33	0.188	–	–	4.034 –	

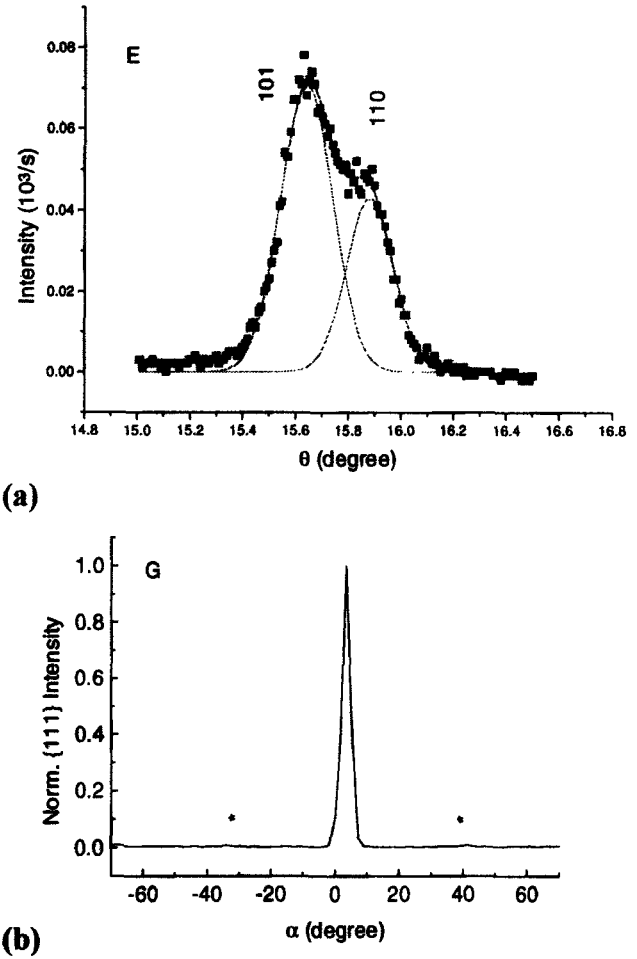

FIGURE 4 (a): Example of a tetragonal-like peak fit, on the (101/110) splitting of sample E. (b): Weak secondary orientation (*) observed on a {111} α-scan ($\alpha = 90 - \chi$) at $\varphi = 0$ for sample G.

FWHMs than PST films. This broadening is associated with at least two effects. Firstly some PZT films are tetragonal, visible as splitting of the 110 cubic peak (101/110), or of 112/211. The 100 peak is at a too low θ angle to reveal a peak separation on our instrument. Similarly, if differences in lattice parameters a and c are too small, a tetragonal refinement was not possible and cubic crystal system was assumed (sample D). In this case the "cubic" cell parameter is shifted towards lower values, and the refinement quality is worse. The broadening may also be due to the poorer crystalline state of

PZT. The {111} reflection, which is not split in the tetragonal system, is appreciably broader than 222-PST at a similar θ angle. Unfortunately, sample H is too strongly textured for observation of the tetragonal splitting or to refine peak positions properly (except 111). However the small "cubic" cell parameter and a very weak 112/211 reflection suggest that the sample is tetragonal. Chromium/gold dots had been deposited on sample G for poling the sample in an electric field. This makes the 111 peak unavailable for refinements, because this peak is overlapped with 111-Au. The cell parameters in all films are close to the bulk values.

For sample B there is only a strong Pt {111} peak in the diffraction pattern, indicative of a strong preferred orientation with ⟨111⟩ directions perpendicular to the underlying Si substrate.

Texture Analysis

1. PST Films

PST

Texture analysis of sample A relied on {220}, {400}, {422} and {620}, pole figures. Figure 5 displays the experimental/normalised and recalculated pole figures. We observed a good agreement, indicative of the high quality of the refinement, and consequently low RP factors (Tab. III). The sample exhibits strong preferred orientation with ⟨100⟩ directions of PST normal to the sample plane, up to a pole density of 18.6 m.r.d. for {100}. Pole figures are not ideally axial but have tetragonal symmetry indicating moderate in-plane orientation. The inverse pole figure of the normal direction (Fig. 6a) shows that there is only a broad 001 maximum corresponding to a 001 texture component. The strength of the PST in-plane alignment can be revealed by the maximum pole density in inverse pole figures (Figs. 6b and 6c) for sample directions marked in Figure 5 as I (parallel to $[10\bar{1}0]$-Al_2O_3 and [0001]-Al_2O_3) and II (at 45° from I) respectively. They show maxima of 5.5 m.r.d., less than a third of the density observed along the normal to the sample plane (18.6 m.r.d.), along ⟨100⟩ -PST and ⟨110⟩-PST with a broad girdle between the two.

Contrary to sample A, on sample B the 222-PST and 111-Pt reflections are partially overlapped (Fig. 3b), and it was not possible to use them in the OD calculation. We observe for this sample (Fig. 7a) a strong preferred orientation of PST with ⟨111⟩ directions at 5° from the normal of the sample surface, but randomly distributed around this direction resulting in a fibre texture. The agreement between recalculated and experimental pole figures for both phases is satisfactory with low RP factors, and the inverse pole

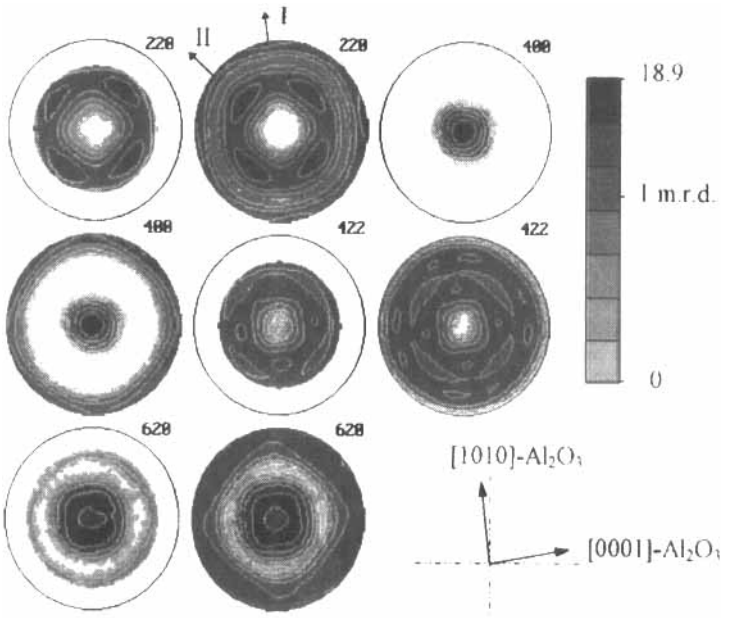

FIGURE 5 Experimental/normalized and recalculated pole figures (successively) of PST in sample A, which show the partial in-plane alignment of PST crystallites, and the quality of the refinement. Substrate in-plane parameters are indicated to identify the alignment. Equal area projection, logarithmic density scale.

TABLE III Refined values of ODF maxima and minima, texture index, entropy and RP factors for all PST, PZT MgO and Pt layers. – indicates that no OD refinement was possible, > 1000 that the value exceeded the program capabilities. {111} maximum pole densities have been calculated by direct integration for the strongest textures of Pt layers, and $\Delta\chi$ gives the FWHM of the {111} texture peak profile

	Layer	{111}; $\Delta\chi$ (*m.r.d.*); (°)	*Min OD* (*m.r.d.*)	*Max OD* (*m.r.d.*)	F^2 (*m.r.d.*)^2	*Entropy*	*RP0* %	*RP1* %
A	PST	⟨100⟩ texture	0	35	10.5	−1.95	14	11
	MgO	–	0.1	8.7	1.4	−0.15	3.5	3
B	PST		0	34	13	−1.97	17	12
	Pt	83;9.1	0	60	13	−1.65	13	13
C	PZT		0.2	4.6	1.4	−0.18	10	8
	Pt	15;9.8	0	34	11	−1.96	18	8
D	PZT		0.7	1.9	1.1	−0.03	1.9	1.9
	Pt	14;11.7	0	174	26	−2.41	38	22
E	PZT		0.30	3.4	1.32	−0.14	9	5
	Pt	366;2.3	–	–	–	–	–	–
F	PZT	37;4.5	0	199	20	−2.18	67	43
	Pt	260;4.3	0	3920	> 1000	−5.9	154	95
G	PZT	62;4	0	43	12	−1.54	41	33
	Pt	124;2.7	0	1360	416	−5.36	109	94
H	PZT	29;3	0	67	24	−2.14	55	35
	Pt	138;3	0	256	227	−5.39	78	55

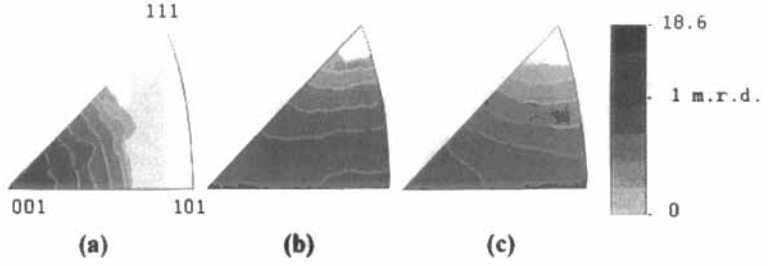

FIGURE 6 Inverse pole figures of PST in sample A for normal direction **(a)**, direction I parallel to $[10\bar{1}0]$-Al_2O_3 **(b)**, and and direction II at 45° from $[10\bar{1}0]$-Al_2O_3 in the substrate plane **(c)**. All crystallites are oriented with c-axes perpendicular to the sample plane. Equal area projection, logarithmic density scale, cubic sector.

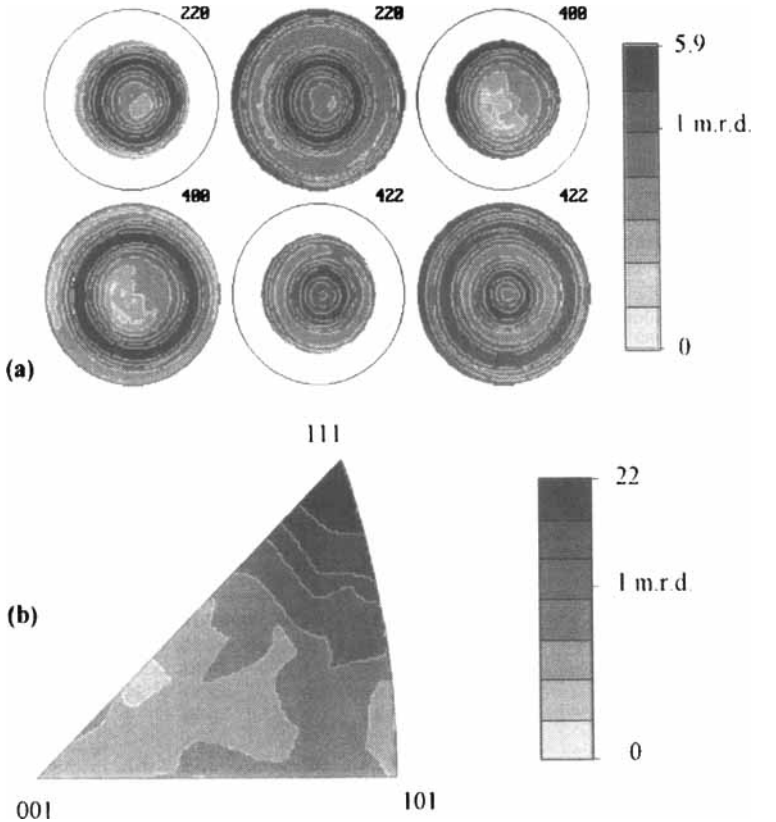

FIGURE 7 **(a)**: Experimental/normalised and recalculated pole figures (successively) of PST in sample B, which show the ⟨111⟩ fibre texture. **(b)**: Inverse pole figure of PST for the normal direction, cubic sector. Equal area projections, logarithmic density scales.

figure of the normal direction (Fig. 7b) only displays the ⟨111⟩ component. The fibre texture has a OD maximum of 34 m.r.d..

Substrates

The MgO buffer layer of Sample A was more difficult to analyse, since the only available peak for texture analysis is 220 (200-MgO is overlapped with 400-PST, and 111-MgO with 311 PST). The {220} pole figure (Fig. 8) shows an in-plane orientation. From this single incomplete pole figure it was possible to calculate an OD. We demonstrated previously[23] for other materials that the WIMV analysis can provide reliable results even if only highly incomplete pole figure data are available. In the case of {220} MgO we were at the limit of the orientation space coverage, yet we obtained fairly low RP factors, and good reproducibility of the {220} pole figure (Fig. 8).

The platinum layer of sample B exhibits the same texture characteristics as the PST film, a 5° tilted ⟨111⟩ fibre texture with only one component, but with a higher orientation density of 60 m.r.d. at maximum.

1. PZT Films

PZT

In all PZT samples, similar to PST sample B, the overlap of 111-PZT and 111-Pt makes these reflections unusable for the OD refinement. Overlap

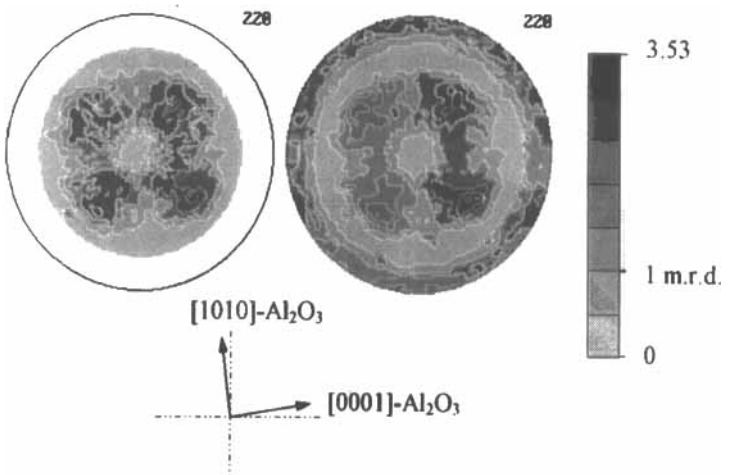

FIGURE 8 {220} experimental/normalised and recalculated pole figures (successively) of MgO in sample A. Equal area projection, linear density scale.

problems also exist between 222-PZT and 311-Pt, and between 200-PZT and 200-Pt. For PZT films we analysed the {100} and {110} pole figures. When the sample appeared to be in the tetragonal phase, we measured the pole figures at the centre of the peaks and determined the OD for cubic symmetry. This assumption did not cause artefacts, nor did it lead to poor refinement quality (RP factors).

The PZT textures can be described as ⟨111⟩ fibres perpendicular to the sample planes, at least for the major component, and for some samples tilted up to 5° from the normal. Figure 9a illustrates the PZT fibre texture of relatively moderate texture strength of film H. The fibre tilt angle is of 2 to 3 degree in this film. Both experimental and recalculated pole figures are shown.

The inverse pole figures for the normal direction of the six PZT layers (Fig. 10a) document the observed fibre textures. Firstly, it is interesting to note that PZT films C and D, each with a thin film of native silicon oxide as one of the buffer layers, exhibit also a ⟨100⟩ component. In both samples, ⟨100⟩ and ⟨111⟩ orientations are of similar magnitude. The texture strength is minimal in sample D (Tab. III). Secondly, PZT films with a thick SiO_2 buffer layer display a strongly prominent ⟨111⟩ texture, samples F, G and H exhibiting the strongest PZT texture. The ⟨111⟩ component increases from E to H. Figure 4b is a χ-scan on the {111} pole figure of sample G, which illustrates the predominance of the ⟨111⟩ component.

Platinum

Figure 9b shows the experimental and recalculated fibre texture of the Pt layer of Sample F, which exhibits the strongest refinable texture in this

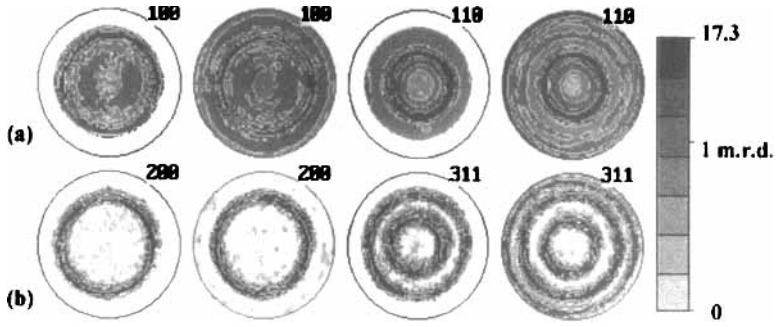

FIGURE 9 Experimental and recalculated normalized pole figures of PZT, sample H **(a)** and Pt, sample F **(b)**. Equal area projections, logarithmic density scale.

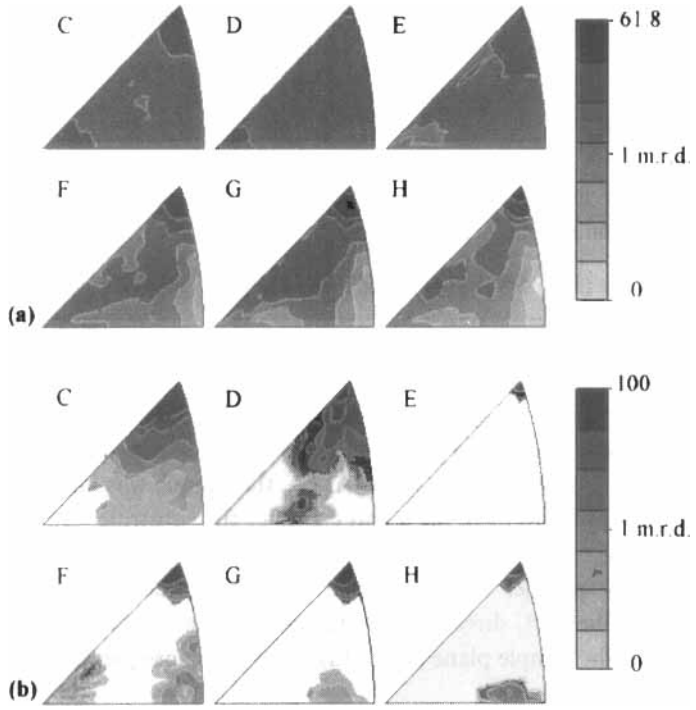

FIGURE 10 Inverse pole figures of PZT (a) and Pt (b) for the normal direction, cubic sector. Equal area projections, logarithmic density scale.

work. Even at such high degree of texture the OD calculation are reasonably good. As for the PZT layers, the fibre tilt angle of Pt ranges from 0 to 5° (like in sample F, Fig. 9b).

For all samples, the texture of the platinum layer (Fig. 10b) is much stronger than that of PZT. On sample F the maximum OD exceeds 3900 m.r.d. This must be interpreted with caution. It may be beyond the resolution of $5°\times5°\times5°$ discrete grid of the OD calculations and produce spurious results. In samples F, G and H there are some secondary components which explain their lower {111} pole density in spite of the narrow {111} texture peak (in comparison with samples E and F). On Sample E, the OD of platinum could not be determined, because of the extremely high texture, which exceeded limitations of our software. However, the {111} pole density, calculated by integration of the pole figures with POFINT, is the highest observed in our samples (366 m.r.d.) and the {111} texture peak was narrower than in all other samples (Tab. III). For instance sample F which exhibits the highest OD and only one

orientation component shows only 260 m.r.d. at the maximum of the {111} texture peak.

DISCUSSION

In all samples except A, the dominant orientation relationships in the normal direction can be described as:

$$\langle 111\rangle\text{-PSTor}\langle 111\rangle\text{-PZT}//\langle 111\rangle\text{-Pt}//[100]\text{-Si}$$

These fibre textures appear with tilt angles up to 5°. While the PZT (or PST) texture always are tilted towards the same azimuth and have a similar tilt angle value as Pt, we noticed no systematic correlation between Pt and the Si substrate. This may be the result of the intermediate deposited layers.

For sample A deposited on $(11\bar{2}0)$-Al_2O_3, the sample was aligned on the goniometer in order to have the **a** and **c** axes of the substrate ($[10\bar{1}0]$-Al_2O_3 and [0001]-Al_2O_3 directions respectively) as indicated in Figure 8 (approximately parallel to the vertical and horizontal pole figure axes respectively). The $\langle\bar{1}01\rangle$ directions of MgO are perpendicular to $\langle 111\rangle$ which are normal to the sample plane (Fig. 11a). They are consequently located on

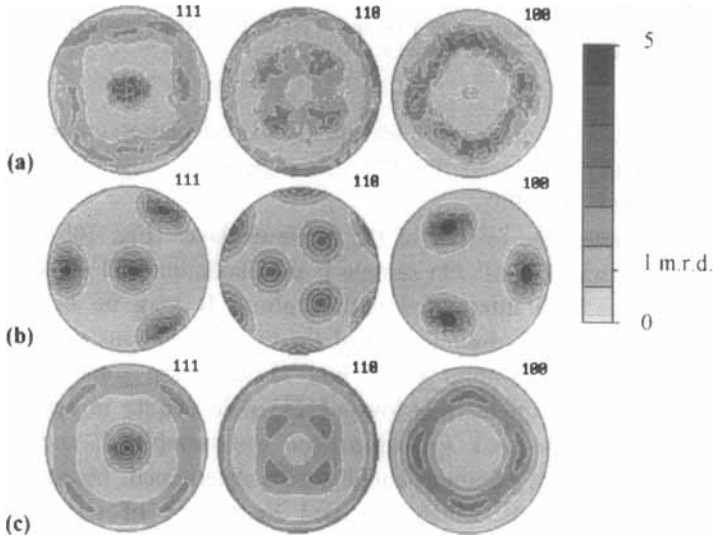

FIGURE 11 {111}, {110} and {100} pole figures of the MgO layer of sample A. **(a)**: Recalculated from the OD. **(b)**: simulated for one of the four components present in the layer, assuming Gaussian of 30° of widths. **(c)**: simulated for the four components. Equal area projections, linear density scale.

the periphery of the {220} pole figure (Fig. 8), for which we observe a slight reinforcement along the $[10\bar{1}0]$-Al_2O_3 and [0001]-Al_2O_3 directions. Then, $\langle\bar{1}01\rangle$-MgO directions align preferentially along the $[10\bar{1}0]$-Al_2O_3 and [0001]-Al_2O_3 axes of the substrate plane. In a MgO single-crystal, the $\langle 110\rangle$ directions are located at 35° to $\langle 111\rangle$, as one can see in the pole figures (Fig. 11b). The alignment of $\langle\bar{1}01\rangle$ with $[10\bar{1}0]$-Al_2O_3 and [0001]-Al_2O_3 gives four statistically equivalent orientations with $\langle 111\rangle$-MgO tilted from the normal. Figure 11 interprets this texture with calculated theoretical pole figures, assuming Gaussian shape orientation components of 30° widths. Figure 11a shows the recalculated {111}, {110} and {100} pole figures for MgO. Figure 11b represents one of the 5° tilted $\langle 111\rangle$ orientations using theoretical pole figures. Figure 11c shows the theoretical pole figures for all four rotated components. There is strong agreement between simulated and experimental pole figures.

The major orientation relationships of this sample can then be summarized as:

$$\langle 100\rangle\text{-PST}//\approx\langle 111\rangle\text{-MgO}//[11\bar{2}0]\text{-}Al_2O_3$$

$$\langle 110\rangle\text{-PST}//\langle 211\rangle\text{-MgO and }\langle 110\rangle\text{-MgO}//[10\bar{1}0]$$
$$\text{and [0001]-}Al_2O_3$$

The mismatch in d-spacings between d_{110}-PST and two d_{110}-MgO is 3.4%, and 0.4% between three d_{220}-PST and five d_{211}-MgO (Fig. 12a).

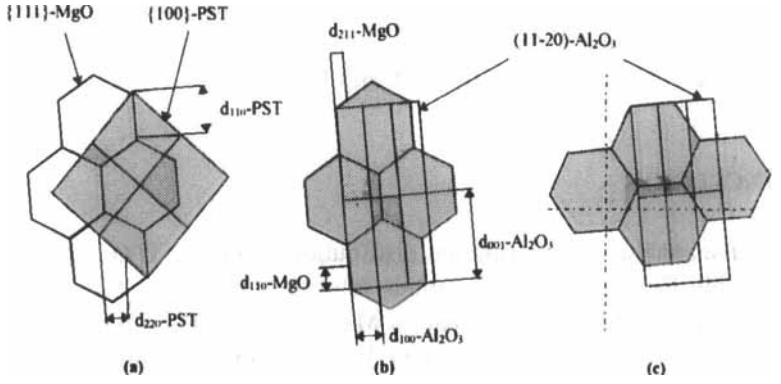

FIGURE 12 Epitaxial relationships for sample A, as deduced from the orientation analysis. Top layers are in gray shade. **(a)**: {100}-PST planes on {111}-MgO, for one orientation of {111}-MgO. **(b)**: first orientation of {111}-MgO plane on $(11\bar{2}0)$-Al_2O_3. **(c)**: second orientation of {111}-MgO planes on $(11\bar{2}0)$-Al_2O_3.

The mismatches between MgO and Al_2O_3 are larger and might explain the larger dispersion of the MgO texture. A first orientation (Fig. 12b) corresponds to coincidences of four d_{110}-MgO d-spacings with d_{001}-Al_2O_3 (8.3% of mismatch), and seven d_{211}-MgO with three d_{100}-Al_2O_3 and a mismatch of 2.6%. A second orientation (Fig. 12c) is due to coincidences of three d_{220}-MgO d-spacings with d_{100}-Al_2O_3 (8.5% of mismatch), and eight d_{211}-MgO with d_{001}-Al_2O_3 with 5.9% of mismatch. Due to the weak mismatch differences between these two orientation, MgO crystallites can choose either orientation with an equal probability. This generates, associated with the fibre tilt, the four-fold symmetry of the texture pattern. Even if the texture of MgO is relatively weak, it produces a PST texture strength (see Entropy and F^2 in Tab. III) comparable to the one obtained with the Pt/Ti/SiO_2 combination, and allows in-plane alignment of low-index crystallographic directions of PST.

Deposition of the platinum layers onto the thin native oxide of the Si substrate results in more dispersed Pt textures and in a multiple component texture in the PZT films. With a thermally grown SiO_2 buffer layer the texture is enhanced in the platinum layer, and to a lesser degree in the PZT films. However, the Zr/Ti ratio considerably modifies the PZT texture. Hence the only sample deposited on Pt/Ti/thermal-SiO_2 with a lower Zr content (sample E) has a similar texture strength and entropy as samples C and D without the thermal oxide buffer. Also sample E presents the strongest Pt texture and the lowest PZT texture. Interestingly, the PZT films on which we observed a tetragonal Bragg peak splitting (samples E and F) are deposited on Pt/Ti/SiO_2 layers, and without much influence of the Zr/Ti composition in this range. Comparing samples E and F (tetragonal PZT) and G and H (cubic PZT), it appears that there is no quantitative texture strength correlation between the PZT and Pt layers.

CONCLUSION

We have analysed the orientation distribution of Pb(Zr, Ti)O_3 and Pb_2ScTaO_6 thin films deposited on various substrates and buffer layers. In the ⟨100⟩ oriented PST film deposited on MgO/(11$\bar{2}$0)-Al_2O_3, a weak in-plane alignment was observed. The MgO buffer exhibits a complex texture, composed of four components. Epitaxial-like relationships with the substrate have been described. The PST film on Pt/(100)-Si exhibits a strong ⟨111⟩ fibre texture, tilted by 5° from the normal. The Pt buffer has the same orientation as PST, with higher orientation densities.

Some PZT films have been stabilised in a tetragonal crystal system, with no apparent correlation to the texture. A ⟨111⟩ fibre texture is observed in all the analysed PZT films, with various texture strength, and in some films untilted. A minor ⟨100⟩ fibre component is present. Using a thermally-grown SiO_2 buffer between Pt and Si favours the stabilisation of the tetragonal PZT phase, and strengthens the Pt texture. The PZT textures also depend on the Zr/Ti content. A decrease in the Zr/Ti ratio weakens the texture. The main texture of the platinum is always of higher strength than that of the PZTs.

Further investigation is required to determine how the texture of such films correlates with ferroelectric properties, and how manufacturing techniques can be optimized to control them. Also, it should be noticed that the texture analyses carried out in this paper assumed centrosymmetry. This is not necessarily the case for non-centric ferroelectrics. The absolute orientation distribution of crystallites could possibly be determined by making use of anomalous scattering, for instance making use of synchrotron facilities, where wavelengths can be varied in the vicinity of absorption edges.

Acknowledgement

One of the author (D. C.) would like to thank the French Ministère de l'Education Nationale, de l'Enseignement Supérieur et de la Recherche (MENESR) for its financial support during his stay at the Dept. of Geology and Geophysics, Berkeley. The supply of PST samples from the Defense Research Agency, Malvern, is gratefully acknowledged. H.-R.W. acknowledges hospitality at the Lab. de Cristallographie, Grenoble, during a sabbatical leave, support through NSF grant EAR 94-17580 and the France-Berkeley Fund.

References

[1] Heidelbach, F., Wenk, H.-R., Muenchausen, R. E., Foltyn, S., Nogar, N. and Rollett, A. D. (1992). *J. Mater. Res.*, **7**, 549.
[2] Pernet, M., Chateigner, D., Germi, P., Dubourdieu, C., Thomas, O., Sénateur, J. P., Chambonnet, D. and Belouet, C. (1994). *Physica C*, **235–240**, 627.
[3] Yoon, D. S., Kim, C. J., Lee, J. S., Lee, W. J. and No, K. (1994). *J. Mater. Res.*, **9**, 420.
[4] Okada, M. and Tominaga, K. (1992). *J. Appl. Phys.*, **71**, 1955.
[5] Warren, W. L., Tuttle, B. A., Schwartz, R. W., Hammmetter, W. F., Goodnow, D. C., Evans Jr, J. T. and Bullington, J. A. (1993). *Proc. MRS Symp. on Ferroelectric Films III*, **310**, 3–8.
[6] Carim, A. H., Tuttle, B. A., Doughty, D. H. and Martinez, S. L. (1991). *J. Amer. Ceram. Soc.*, **74**, 1455.

[7] Seraphin, S., Zhou, D., Teowee, G., Boulton, J. M. and Uhlmann, D. R. (1993). *Proc. MRS Symp. on Ferroelectric Films III*, **310**, 369–374.
[8] Whatmore, R. W., Huang, Z., Todd, M. and Watton, R. (1997). submitted.
[9] Reaney, I.M., Patel, A. and Barber, D. J. (1992). *Brit. Ceram. Proc.*, **44**, 251.
[10] Patel, A. and Obhi, J. S. (1995). *GEC J. Res.*, **12**(3), 141.
[11] Baba-Kishi, K. Z., Cressey, G. and Cernik, R. J. (1992). *J. Appl. Cryst.*, **25**, 477.
[12] Huang, Z., Todd, M., Watton, R. and Whatmore, R. W. (1997). Submitted.
[13] Liu, D. and Payne, D. (1995). *J. Appl. Phys.*, **77**, 3361.
[14] Schulz, L. G. (1949). *J. Appl. Phys.*, **20**, 1030.
[15] Rodriguez, J., Anne, M. and Pannetier, J. (1992). *STRAP, a System for Time-Resolved Data Analysis (Powder Diffraction Patterns)*, ILL Grenoble Int. Rept.
[16] Wenk, H. -R., Sintubin, M., Huang, J., Johnson, G. C. and Howe, R. T. (1990). *J. Appl. Cryst.*, **67**, 572.
[17] Chateigner, D., Germi, P. and Pernet, M. (1992). *J. Appl. Cryst.*, **25**, 766.
[18] Matthies, S. and Vinel, G. W. (1982). *Phys. Stat. Sol. B.*, **112**, K111.
[19] Matthies, S., Vinel, G. W. and Helming, K. (1987). *Standard Distributions in Texture Analysis* (Akademie-Verlag Berlin).
[20] Bunge, H. J. (1982). *Texture Analysis in Materials Science* (Butterworths, London).
[21] Matthies, S., Helming, K. and Kunze, K. (1990). *Phys. Stat. Solid B*, **157**, 489.
[22] Wenk, H.-R., Matthies, S., Donovan, J. and Chateigner, D. "BEARTEX, Berkeley Texture Package", accepted to *J. Appl. Cryst.*
[23] Chateigner, D., Wenk, H.-R. and Pernet, M. (1997). *J. Appl. Cryst.*, **29**, 2.